Reconditioning Criteria of Wheel Profiles based on the Rolling Radius Difference

Fujie Xia and Colin Cole
Rail CRE, Faculty of Sciences, Engineering and Health, Central Queensland University, North Rockhampton, QLD 4702, Australia

Summary: Wheel rail rolling contact plays a key role for the stability of wagons on straight track and their capacity to negotiate through curves. After a certain period of operation the profiles of wheel and rail become worn, losing original designed form. In the general case the right and left wheel radii may not remain identical which gives a rolling radius difference. At some point in time, reconditioning work is arranged to return the wheel to its original profile. This paper explores the effects of the rolling radius difference on the performance of the complete wagon system and uses the results to be as a reference for determining a maintenance criterion for wheel reconditioning.

Index Terms: Wheel rail profiles; Rolling radius difference; Equivalent conicity.

1. INTRODUCTION

The motion state of railway wagon is strongly dependent on the wheel-rail reaction forces. Wheel rail rolling contact plays a key role for the stability of the wagon on straight track and the capacity of it to negotiate through curves. The profiles of wheel and rail control wheel rail contact reaction forces. After a certain period of operation the profiles of wheel and rail become worn, loosing original designed form. In the general case the right and left wheel radii will be difficult to keep identical and radius differences will appear. At some point in time, reconditioning work is arranged to return the wheel to its original profile. In the process the wheel radius is decreased.

If a wheel radius difference exists, the roll angle of wheelset is nonzero for the central wheelset position and the equivalent conicity is also changed. As a consequence result, lateral motion of wagon will take place resulting in an offset position on straight track. For larger wheel radii difference it will cause flange contact. This paper focuses on the effect of rolling radius difference on the motion of railway wagon with three-piece bogie.

The simulations were completed with a model of a typical freight wagon with 3 piece bogies: (i.e. 11 masses: 1 wagon car body, 2 bolsters, 4 side frames and 4 wheelsets). The wagon is modeled with non-linear connections and friction elements including two-dimensional dry friction for the side frame and adapter connection and suspension wedge dampers. The two-dimensional dry friction is modelled with stick-slip modes.

In this study, firstly, the effects of wheel radii on wheel rail geometrical contact parameters are investigated. Two and three dimensional cases are included. Then we use a complete wagon model with 66DOFs to analyze the effects on the dynamic performance of wagon on various tracks.

For the wheel profile design it should meet a good stability for wagon on straight track and good smooth performance for wagon through curved track. Generally low equivalent conicity is suitable to the requirement of straight stability and high equivalent conicity is then suitable to the curve through ability. Traditional way to determine equivalent conicity is that uses the two wheel rolling radii difference being divided by the lateral displacement of the corresponding wheelset. The new and more accurate method has been suggested by UIC [1]. This new method was selected in this study and implemented into computer program WRKIN [2].

To find the effect of various levels of wheel radius difference on the wagon motion, various values are investigated for right and left wheel radii with designed and worn profiles. Wagon runs are simulated on both straight track and through curved track and results are discussed.

2. THE WHEEL RAIL GEOMETRICAL CONTACT PARAMETERS FOR DIFFERENT RIGHT AND LEFT WHEEL RADII

In the general case the wheel and rail profiles have shapes differing from the design profile due to wear. In order to determine the wheel rail contact points, the geometrical contact parameters the profiles of a wheel and rail must be first known. Normally worn profiles of left/right wheels are asymmetrical and accurate vehicle dynamics simulation requires actual profile measurements.

It is not possible to obtain an analytical solution for the kinematical constraints with arbitrary wheel and rail profiles, so numerical methods are needed.

Both B-Spline curve fitting method and piece-wise curve fitting method[2] are selected for fitting the profile data. They are implemented into computer program WRKIN[2]. The B-Spline curve fitting method is for new profile and piece-wise curve fitting is then for measured profiles.

The wheel rail contact point is found through determining the minimal distances between the two surfaces of the left and right wheels and the corresponding rail profiles for various roll angles and lateral displacements of the wheelset. After finding the contact point the corresponding geometrical contact parameters can be determined. For three-dimensional geometric contact problem, a two dimensional search on the surface of the wheel in the longitudinal and lateral directions is needed, so the computational time is high. Alternative method is to replaces the surface of the wheel by the so-called trajectory on the tread of the wheel. The minimal distance comparison is processed between the trajectory and the profile of a rail [3], so the spatial curve surface is simplified to a spatial line.

The equivalent conicity plays an essential role since it allows the satisfactory appreciation of the wheel-rail contact on tangent track and on large-radius curves. The term equivalent conicity is now used in a number of standards documents, including UIC leaflets[1], ISO standards and European standard, so it is necessary to correctly determine it.

The traditional way for calculating equivalent conicity is taking the difference of the two wheel rolling radii difference dividing by the lateral displacement, i.e.,

$$\tan\gamma_e = \frac{\Delta r}{2y}, \tag{1}$$

where Δr denotes the left/right wheel rolling radii difference and y is the lateral displacement of wheelset.

In the recent UIC publication suggested an unambiguous way of determining the equivalent conicity as followings. The equation of motion of a wheelset on track can be expressed on the basis of the yaw angle [1]

$$\frac{d\psi}{dy} = -\frac{\Delta r}{e r_0 \Psi}, \tag{2}$$

where e is the distance between the left and right contact points; r_0 stands for the radius of the wheels when the wheelset is centred on the track; and ψ is the angle of the wheelset movement in the x-y-plane and determined by

$$\Psi = \sqrt{\frac{-2}{e r_0}\left[\int \Delta r dy + C\right]} \tag{3}$$

Where the constant C is determined by the way such that $\psi_{e\min} = 0$ for the corresponding, $y_{e\min}$.

The wheelset's movement on the track is then obtained with the help of the following integration:

$$\frac{dy}{dx} = \frac{1}{\psi}. \tag{4}$$

From Eqns. (2)-(4), the Klingel motion can be obtained as

$$x = \int \frac{1}{\sqrt{\frac{-2}{e r_0}\left[\int \Delta r dy + C\right]}} dy \tag{5}$$

between $y_{e\min}$ and $y_{e\max}$, which allows determination of the wavelength λ of the wheelset's kinematical motion. To the end the equivalent conicity is determined by the Klingel formula

$$\tan\gamma_e = \left(\frac{\pi}{\lambda}\right)^2 2 e r_0. \tag{6}$$

From the above analysis the contact parameters such as roll of wheelset, equivalent conicity are affected by wheel radius. Different left/right wheel radii will produce different results.

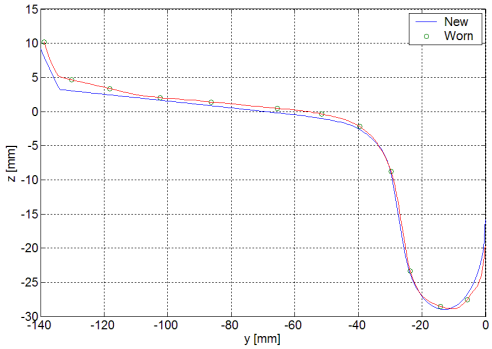

Figure 1. New and light worn QR LW2 profiles

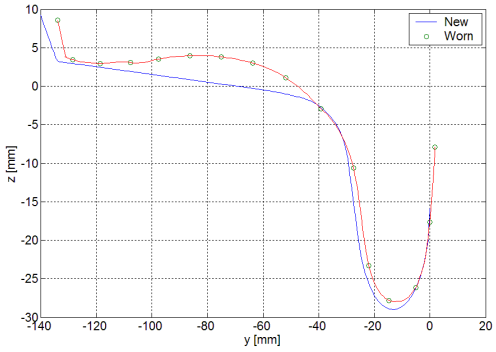

Figure 2. New and heavy worn QR LW2 profiles

The profiles of Queensland wheel LW2 and QRAS60 rail are used for the investigation. The gauge is 1067 mm in Queensland rail. The inclination of the rail is 1:20. The Figures 1 and 2 show the comparisons of new and worn wheel profiles, respectively.

Figure 3 shows the distribution of wheel rail contact points with radius differences, $\Delta r = 5$mm, with new wheel profiles. For this combination of wheel and rail profiles the contact point distributions don't cover long segments of rail profile. If the left wheel radius is increased the left wheel flanging area decreases and the wheel flanging area increases. Figure 4 shows the distribution of wheel rail contact points with radius difference, $\Delta r = 4$mm, with heavy worn wheel profiles. For this form of worn profiles the wheel rail contact point distribution areas are is increased. As the two worn profiles differ this adds a further dimension of difficulty to the analysis.

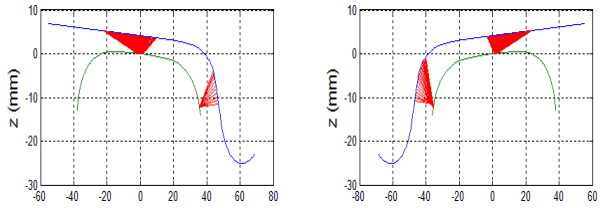

Figure 3. Wheel rail contact points change with left-right wheels radii difference, $\Delta r = 5$mm, new profiles.

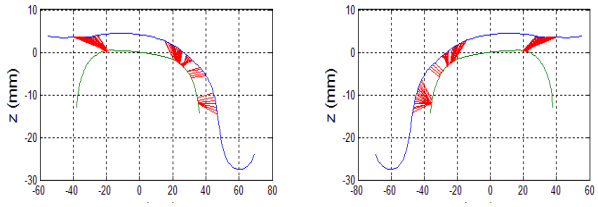

Figure 4. Wheel rail contact points change with left-right wheels radii difference, $\Delta r = 4$mm, heavy worn profiles.

Figures 5. shows the change in roll angle of the wheelset with radius difference illustrating why the wagon has lateral displacement even running on perfect straight track.

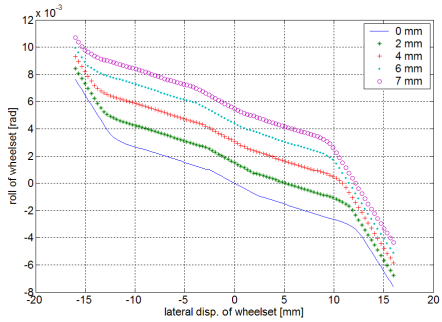

Figure 5. Roll of wheelset vs lateral displacement of the wheelset, heavy worn wheel.

Figure 6 and 7 show the equivalent conicity change with new and heavy worn profiles for wheel radius differences from 0 to 6mm. In both plots the left wheel radius is larger than the right one. Note the equivalent conicity changes are different for the new and worn profiles.

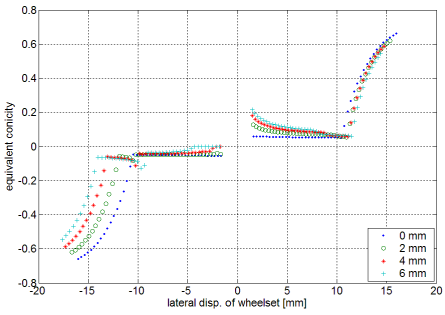

Figure 6. Equivalent conicity change, left radius larger, new profiles.

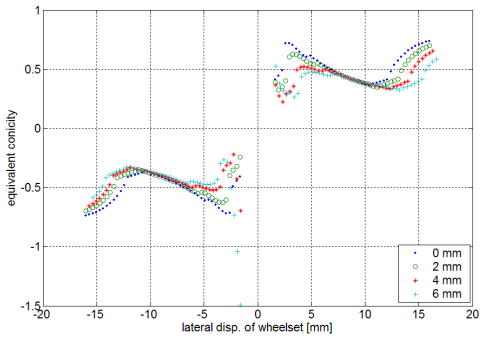

Figure 7. Equivalent conicity change, left radius larger , heavy worn profiles.

3. A COMPLETE WAGON MODEL

The simulations were completed with a model of a typical freight wagon with 3 piece bogies: (i.e. 11 masses: 1 wagon car body, 2 bolsters, 4 side frames and 4 wheelsets). Each mass was modeled with 6 degrees of freedom making for a total 66 degrees of freedom for a wagon system. The simulation package was the C66 wagon simulation code developed in-house as part of Project #1 for the Australian Rail CRC.

The equation of wagon system can be written as

$$[M]\ddot{X} = F_n + F_t + F_w + F_g + F_c + F_d + F_s - F_f \quad (7)$$

The symbols in equation are below:

M : System mass matrix
F_n : Normal wheel rail contact force vector
F_t : Tangential wheel rail contact force vector
F_w : Weight vector
F_g : Gyroscopic force vector
F_c : Centrifugal force vector
F_d : Damping force vector
F_s : Spring force vector
F_f : Friction force vector

The kinematical wheel rail contact parameters were calculated prior to simulation by the program WRKIN to form the wheel rail contact table which includes the static wheel normal force, Kalker creep coefficients and the dimensions of contact ellipse as a function of the lateral displacement of the wheelsets. The wheel rail contact parameter table is then used as a look-up table during the simulation. The effective normal wheel force can be determined by [2]:

$$F_{nd} = \left(F_{n0}^{\frac{2}{3}} + K_h^{\frac{2}{3}} q_d\right)^{\frac{3}{2}} \quad (8)$$

Where q_d is dynamic penetration, F_{n0} stands for static wheel load and K_h is Hertzian spring stiffness. The dimensions of the contact ellipse are then given by[2]

$$a_d = a_0\left[\frac{F_{nd}}{F_{n0}}\right]^{\frac{1}{3}}, b_d = b_0\left[\frac{F_{nd}}{F_{n0}}\right]^{\frac{1}{3}}, a_d b_d = a_0 b_0\left[\frac{F_{nd}}{F_{n0}}\right]^{\frac{2}{3}} \quad (9)$$

where a_0, b_0 is the dimension of elliptic contact area to the static wheel load, F_{n0}. With the known contact dimension the tangential wheel rail contact force can be determined with creepages

$$\begin{aligned} \nu_{xj} &= 1 - (r_w\dot{\theta} - \dot{x} \mp b\dot{\psi})/V \mp b\kappa \\ \nu_{yj} &= -\psi\cos^{-1}\gamma_j + (\dot{y} - r_w\dot{\varphi})/V\cos\gamma_j \\ \phi_{sj} &= \mp\sin\gamma_j / r_w + \dot{\psi}\cos\gamma_j / V \end{aligned} \quad (10)$$

Where r_w stands for wheel rolling radius, $\dot{x}, \dot{y}, \dot{\theta}, \dot{\psi}$ is longitudinal, lateral speed, pitch perturbation angular speed and raw speed, respectively. b stands for half spacing between left and right wheel rail contact points, κ is the curvature of curved track, and γ stands for wheel rail contact angle. Taking upper of '$\mp$' for $j = 1$ which stands for right wheel and lower of '$\mp$' for $j = 2$ which stands for left wheel.

From Kalker's linear theory[5] the tangential wheel rail contact forces and torque in yaw can be written

$$\begin{bmatrix} T_X \\ T_y \\ M_z \end{bmatrix} = -Gc^2\begin{bmatrix} C_{11} & 0 & 0 \\ 0 & C_{22} & cC_{23} \\ 0 & -cC_{23} & c^2C_{33} \end{bmatrix}\begin{bmatrix} \nu_x \\ \nu_y \\ \varphi_s \end{bmatrix} \quad (11)$$

Where G is shear modulus, C_{ij} stands for Kalker creep coefficients and c is the square root of the product of radii of the elliptic wheel rail contact area. The resultant force can be written as [6]

$$T_r^* = \sqrt{T_x^2 + T_y^2}, \quad (12)$$

Let $u = T_r^* / \mu F_{nd}$ then

$$T_r = \mu F_{nd}\begin{cases} u - u^2/3 + u^3/27, & T_r^* < 3\mu F_{nd} \\ 1, & T_r^* \geq 3\mu F_{nd} \end{cases} \quad (13)$$

Finally the approximation of the nonlinear longitudinal and lateral creep forces is

$$T_x^* = \frac{T_x}{T_r^*} T_r, \quad T_y^* = \frac{T_y}{T_r^*} T_r \tag{14}$$

Iteration algorithm was used to obtain accurate normal and tangential wheel rail contact forces. Friction force can be determined by [7]

$$F_f = \begin{cases} k_s \Delta d, & |k_s \Delta d| \le F_{fs} \ \& \ |v_r| \le \delta v_r, \\ F_{fs}, & |k_s \Delta d| > F_{fs} \ \& \ |v_r| \le \delta v_r, \\ F_{fk}, & |v_r| > \delta v_r. \end{cases} \tag{15}$$

Where $F_{fs} = N\mu_s sign(\Delta d)$ stands for static friction force; $F_{fk} = N\mu_k sign(v_r)$ is kinetic friction force; Δd stands for resultant relative displacement and v_r is relative velocity and δv_r stands for a small value of relative velocity for numerical analysis requirement. Static and kinetic friction coefficients are represented by μ_s and μ_k, respectively.

For the two-dimensional case the components of friction forces in *x* and *y* directions from Eq. (15) are:

$$F_{fx} = \begin{cases} k_s \Delta d_x, & k_s \Delta d \le F_{fs} \ \& \ |v_{rs}| \le \delta v_r, \\ F_{fs} \Delta d_x / \Delta d, & k_s \Delta d > F_{fs} \ \& \ |v_{rs}| \le \delta v_r, \\ F_{fk} v_{rx} / v_{rs}, & |v_{rs}| > \delta v_r. \end{cases} \tag{16}$$

$$F_{fy} = \begin{cases} k_s \Delta d_y, & k_s \Delta d \le F_{fs} \ \& \ |v_{rs}| \le \delta v_r, \\ F_{fs} \Delta d_y / \Delta d, & k_s \Delta d > F_{fs} \ \& \ |v_{rs}| \le \delta v_r, \\ F_{fk} v_y / v_{rs}, & |v_{rs}| > \delta v_r. \end{cases} \tag{17}$$

Where $\Delta d, v_{rs}$ are defined by

$$\Delta d = \sqrt{\Delta d_x^2 + \Delta d_y^2}, \quad v_{rs} = \sqrt{v_{rx}^2 + v_{ry}^2} \tag{18}$$

and for this case $F_{fs} = N\mu_s$ and $F_{fk} = N\mu_k$.

4. CASES STUDIES

In the case studies, the running speed is 20m/s and the wagon is loaded, wagon body mass is 66 tonnes.

The straight track with track irregularities and curved tracks are used for the simulation. For the straight track class 5 irregularity track from PSD plots[8] was used. The radius of the curved track is 1000m and the super elevation of out side rail was 35mm with 60 m transients.

4.1 Irregularity track using new profiles

Figure 8 shows the lateral displacement of the first wheelset comparing $\Delta r = 0$ and $\Delta r = 2$mm. Figure 9 the comparison of right lateral wheel rail contact forces.

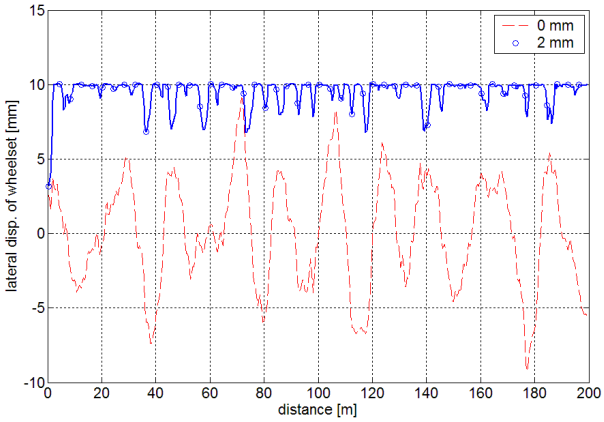

Figure 8. Lateral displacement of the first wheelset, new profile

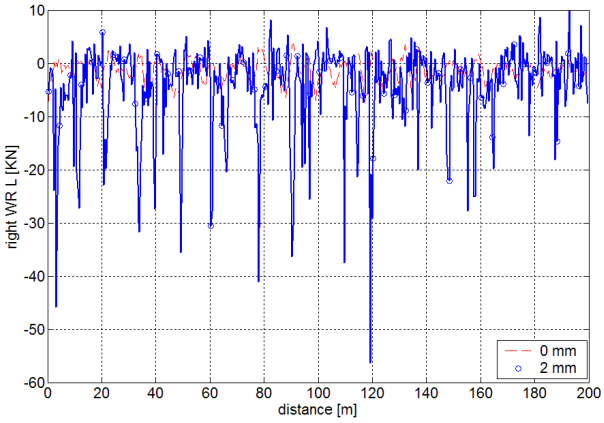

Figure 9.Right wheel rail contact force of the first wheelset

4.2. Irregularity track using heavy worn profiles

Figure 10 shows the lateral displacement of the first wheelset comparing $\Delta r = 0$ and $\Delta r = 3$mm. Figure 11 the comparison of left lateral wheel rail contact forces .

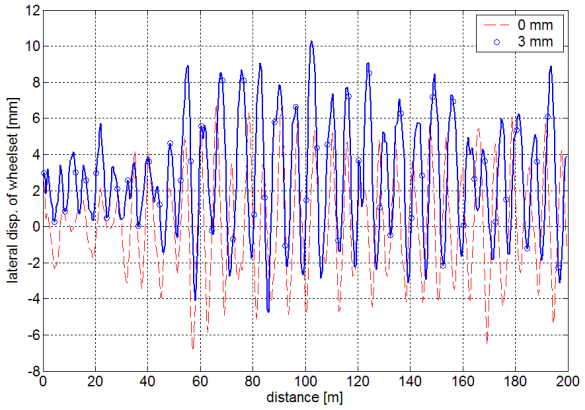

Figure 10. Lateral displacement of the first wheelset

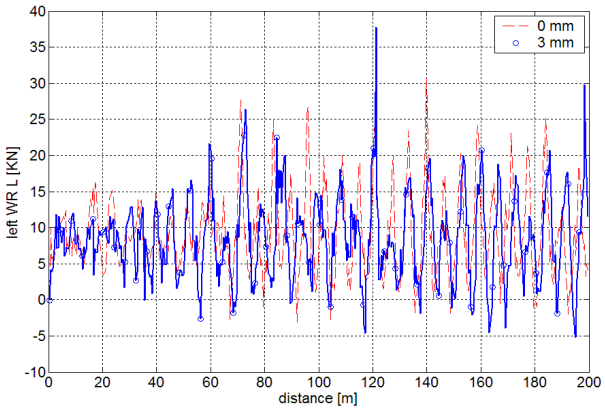

Figure 11. Lateral wheel rail contact force of the first wheelset

4.3. Irregularity track using light worn profiles

Figure 12 shows the lateral displacement of the first wheelset comparing $\Delta r = 0$ and $\Delta r = 2$mm. Figure 13 the comparison of right lateral wheel rail contact forces.

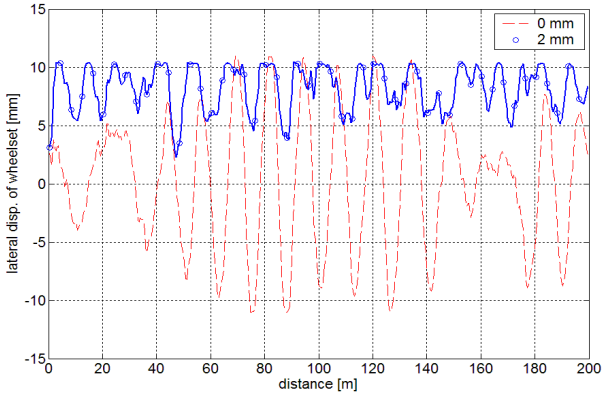

Figure 12. Lateral displacement of the first wheelset, light worn profile

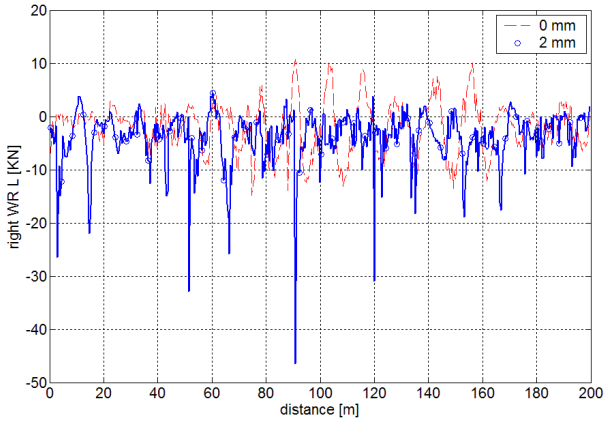

Figure 13. Right wheel rail contact force, light worn profile

4.4. Curved track using new profiles

Figure 14 shows the lateral displacement of the first wheelset comparing $\Delta r = 0$ and $\Delta r = 1$mm. Figure 15 the comparison of right lateral wheel rail contact forces.

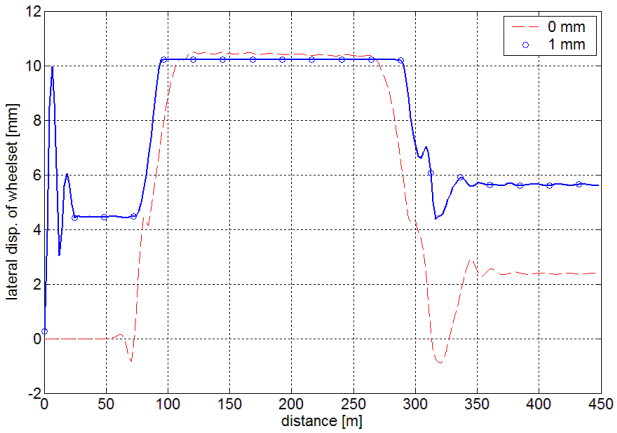

Figure 14. Lateral displacement of the first wheelset

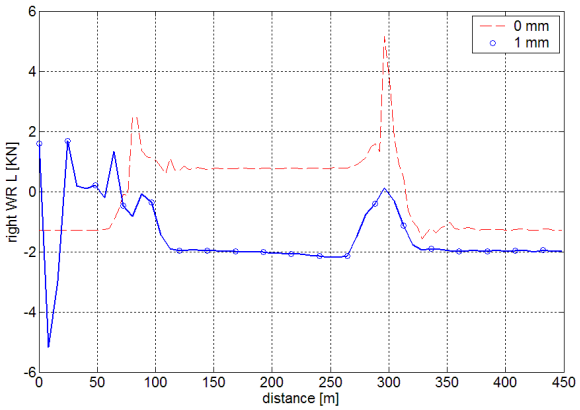

Figure 15. Right wheel rail contact force of the first wheelset

4.5. Curved track using heavy worn profile

Figure 16 shows the lateral displacement of the first wheelset comparing $\Delta r = 0$ and 4mm. Figure 17 the comparison of right lateral wheel rail contact forces.

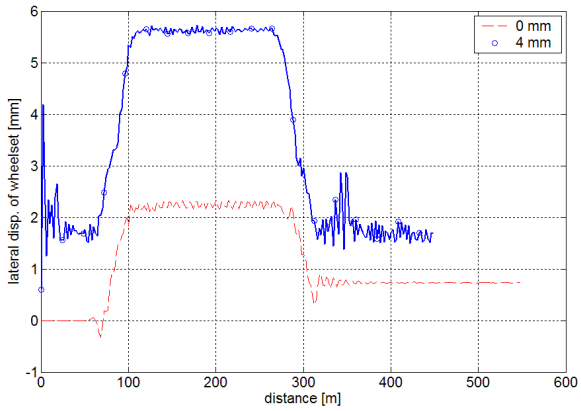

Figure 16. Lateral displacement of the first wheelset

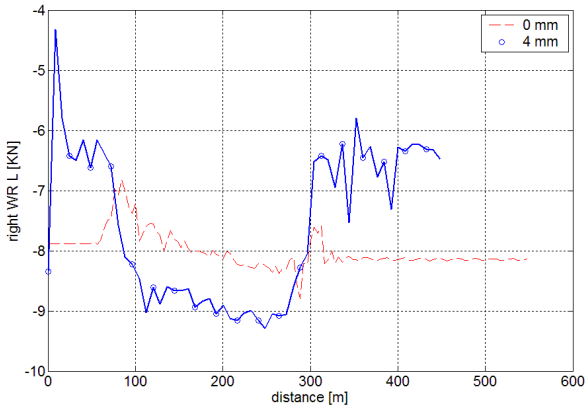

Figure 17. Lateral vertical wheel rail contact force of the first wheelset

4.6. Curved track using light worn profile

Figure 18 shows the lateral displacement of the first wheelset comparing $\Delta r = 0$ and 1mm. Figure 19 the comparison of right lateral wheel rail contact forces.

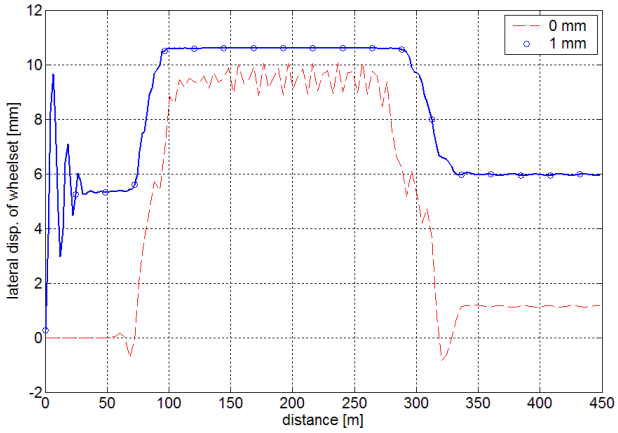

Figure 18. Lateral displacement of the first wheelset

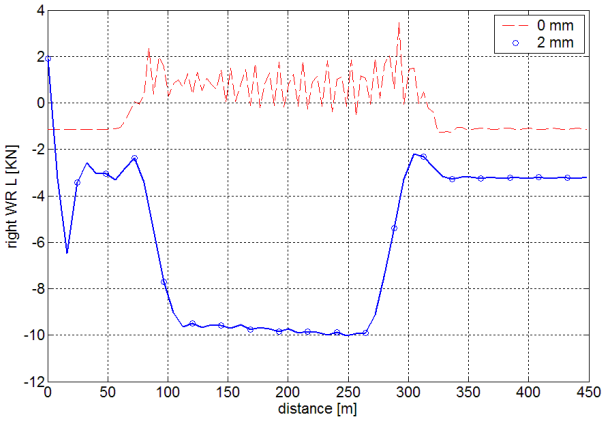

Figure 19. Right lateral wheel rail contact force of the first wheelset

4.7. Left uses light worn profile and right new profile

Figure 20 shows the lateral displacement of the first wheelset comparing of new and light worn wheel profiles. Figure 21 the comparison of right lateral wheel rail contact forces with left light worn and right new wheel profiles.

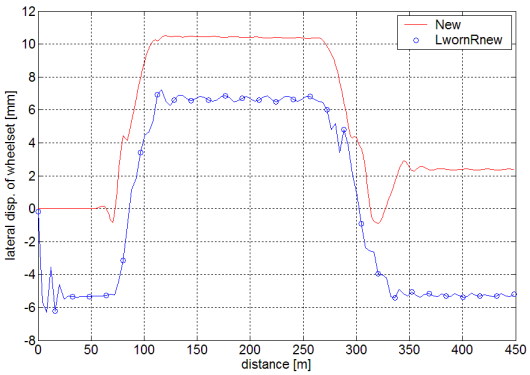

Figure 20. Left lateral wheel rail contact force of the first wheelset

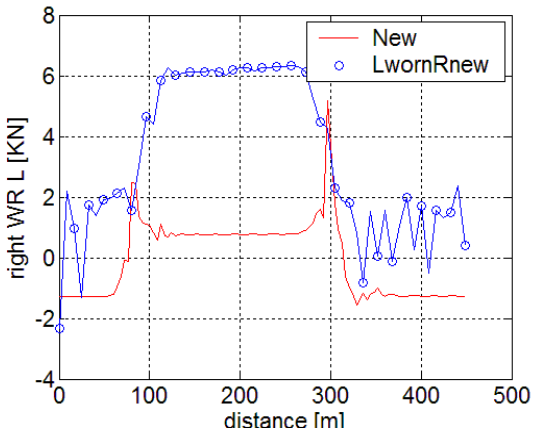

Figure 21. Right lateral wheel rail contact force of the first wheelset

5. DISCUSSION

The simulation of wheelsets with different diameter wheels offers an objective method of determining the implications of wheel radius differences. This work is in its early stages and only very limited results are shown in this paper (e.g. only one curve case and only mild track irregularity, FRA Class 5). Of interest is the new draft Australian Code of Practice [9] which has set wheelset tread radius difference at 1mm. The results in Figure 8 show persistent flange contact on relatively mild Class 5 track irregularity with 2mm radius difference or 4 mm diameter difference. Lateral forces are likewise on concern, Figure 9. The results in Figure 10 and 11, with heavily worn profiles show much less dependence on an even larger wheel radius difference, e.g. 3mm. It would appear that the worn profiles have resulted in hunting in which the wheelset radius difference has resulted only in an offset of the centred position. Wheel profiles with less wear as shown in Figure 12 and 13 give similar results to that of new profiles in Figures 8 and 9.

Curved track results show earlier onset of flange contact in Figure 14 and considerable cost in lateral wheel forces, (hence wear) in Figure 15. Note that the radius difference is only 1mm (e.g. diameter difference of 2mm) and the curvature radius in 1000m. Again the heavily worn profiles give less severe results in Figure 16 and 17 and lightly worn results being similar to new, Figures 18 and 19.

The further study of new and slightly worn profiles on the same wheelset, figure 20 and 21, show the marked effect of asymmetry in wheelset performance.

As can be seen by the discussion above, different combinations of wheel wear and wheel radius difference can give quite different results. The simulation work is in early stages but these results indicate that a performance based criteria could be possible for determining wheelset condition limits.

6. CONCLUSIONS

Wheel radius difference will cause the changes in the roll angle of the wheelset and the equivalent conicity. Equivalent conicity changes are also different for the new and worn profiles.

The effects of rolling radius difference of the wheels on the motion of wagon system are obvious. If radius difference exists the wheelset will track at a position offset from the track centre.

Simulations showed that the maximum lateral and vertical wheel rail contact forces increase with the augment of radius difference.

The paper provides a method of evaluating the effects of the radius difference on the performance of wagon system dynamics. This work is in its early stages and only includes a limited number of cases (new and two(2) worn). More extensive study is necessary.

The results indicate that a performance based criteria, with associated cost benefits, could be possible for determining wheelset condition limits.

ACKNOWLEDGEMENTS

The paper is supported by the Cooperative Research Centre for Railway Engineering and Technologies of Australia (Rail CRC) Theme1: Smart Train System. The work is also obtained support from the Centre for Railway Engineering at Central Queensland University.

REFERENCES

[1] UIC Code 519, Method for determining the equivalent conicity, August, 2002.
[2] Fujie Xia, The Dynamics of the Tree-piece-freight Truck, PhD. Thesis, Informatics and Mathematical Modelling, the Technical University of Denmark, 2002.
[3] K. Wang, On the Geometrical Contact between a Wheel and a Rail(in Chinese), Journal of Southwest Jiaotong University, (1984)1:89-98.
[4] Fujie Xia, Colin Cole and Peter Wolfs, The effects of the friction between frame and adapters on the performance of three-piece truck, Proceedings of ASME/Joint Rail Conference, April 4-6, 2006, Atlanta, Georgia.
[5] J.J. Kalker, Three-Dimensional Elastic Bodies in Rolling Contact, Kluwer Academic Publishers, 1990.
[6] Z.Y. Shen, J.K.Hedrick, J.A. Elkins, A comparison of alternative creep-force models for rail vehicle dynamic analysis, Proceedings of the 8th IAVSD Symposium, MIT, Cambridge, MA, 1984.
[7] Fujie Xia, Colin Cole and Peter Wolfs, The dynamic wheel-rail contact stresses for wagon on various tracks, the proceedings of 7th International Conference on contact Mechanics and Wear of Rail/Wheel Systems, Brisbane, Australia, 2006.
[8] F. Xia, C. Cole, P. Wolfs and D. Roach, Method for Generating Track Irregularity Data from Power Spectral Density Plots, the Workshop of Rail CRC, Theme 1 “Smart Train” Intelligent System, 10 June 2003, Rockhampton, pp.24-30.
[9] Roll 17-2 Wheelsets - Freight 24 Apr 06, http://www.ara.net.au/